

## Self-Organized Monolayer of Nanosized Ceria Colloids Stabilized by Poly(vinylpyrrolidone)

Rui Si,<sup>†</sup> Ya-Wen Zhang,<sup>\*,†</sup> Li-Ping You,<sup>‡</sup> and Chun-Hua Yan<sup>\*,†</sup>

State Key Lab of Rare Earth Materials Chemistry and Applications and PKU-HKU Joint Lab on Rare Earth Materials and Bioinorganic Chemistry and Electron Microscopy Laboratory, Peking University, Beijing 100871, China

Received: December 24, 2005; In Final Form: February 7, 2006

Four nanometer colloidal ceria nanocrystals in a fluorite cubic structure have been synthesized via an alcohothermal treatment at 180 °C for 24 h from  $\text{Ce}(\text{NO}_3)_3 \cdot 6\text{H}_2\text{O}$  in ethanol, using various alkylamines including triethylamine, butylamine, and hexadecylamine as the bases and poly(vinylpyrrolidone) (PVP) as the stabilizer. They were characterized by multiple measurements of X-ray diffraction (XRD), transmission electron microscopy (TEM), high-resolution TEM (HRTEM), ultraviolet visible (UV–vis) spectroscopy, dynamic light scattering (DLS), and infrared spectroscopy (IR). The introduction of PVP could effectively stabilize the cerium nuclei against self-aggregation and finally lead to the formation of the  $\text{CeO}_2$  colloids. As compared with that of their precipitated counterparts, the UV–vis spectra showed a blue-shifted absorption edge for the as-obtained colloidal nanocrystals, revealing that their surfaces were well-passivated by PVP. Four types of self-organized monolayer patterns (i.e., isolated particles, short chainlike (pseudo-1-D aggregated), pearl necklace-like (1-D aggregated), and dendritic (pseudo-2-D aggregated) alignments) appeared for the as-obtained colloidal particles on the copper TEM grids, due to the delicate balance of the attractive and repulsive forces between the PVP-passivated  $\text{CeO}_2$  nanocrystals during the irreversible evaporation of the solvent from various colloidal solutions under ambient conditions. The type of alkylamine and the concentration of PVP were confirmed to be the crucial factors determining the oriented-aggregation dimensionality of the  $\text{CeO}_2$  colloids. Possible interparticle interaction modes have been suggested to explain such complex self-organization patterns exhibited by the as-obtained  $\text{CeO}_2$  nanocrystals.

## Introduction

Recently, nanostructured functional materials have attracted much research interest not only due to their remarkable size-, shape-, or surface-dependent physical and chemical properties but also because of their diverse self-assembled patterns onto multiple substrates in the field of nanodevices. For instance, colloidal semiconductor ( $\text{CdSe}$ ,  $\text{ZnS}$ , etc.) nanocrystals have been synthesized in a controllable manner and are used as luminescent probes or biomarkers in biology and medicine after surface modification.<sup>1,2</sup> Several alterations were employed to directly synthesize the colloidal nanoparticles by using hydrophilic surfactants in polar solvents and thus to avoid the surface-exchange procedure. Among them, hydrothermal or solvothermal routes, particularly powerful for metal oxide systems, take many advantages of one-step, easy operation, and good repetition. Meanwhile, some groups have focused on the investigation of superstructures and/or superlattices due to the self-assembly of the previous colloidal nanoparticles from theoretical simulation to experimental fabrication and microcosmic explanation of the mono- or multiple-layer patterns.<sup>3–11</sup> Up to now, it is still a great challenge for us to control and realize various self-organization modes of nanostructured building blocks from 0-D to 3-D to obtain better fundamental understanding of the complex self-organization phenomenon in the nanometric scale and to reveal further the underlying self-organization principles.

As one of the most important rare earth oxides, ceria ( $\text{CeO}_2$ ) has been extensively applied in catalysis,<sup>12,13</sup> electrochemistry,<sup>14,15</sup> and optics<sup>16,17</sup> due to its unique properties. For example, ceria-based materials have strong absorption in the ultraviolet range and can act as an anti-ultraviolet reagent to protect human skin.<sup>17</sup> In this application,  $\text{CeO}_2$  ultrafine powders were normally used after being surface-coated and redispersed in aqueous solution. As we know, the successful synthesis of colloidal  $\text{CeO}_2$  nanocrystals has been reported in some literature.<sup>18–24</sup> For example, Matijević et al. reported in 1988 the preparation of the dispersions containing polycrystalline  $\text{CeO}_2$  spheres with a uniform size in micrometers via forced hydrolysis of cerium salts in acidic solutions.<sup>18</sup> Chane-Ching obtained aqueous dispersions of nanometric  $\text{CeO}_2$  particles by hydrolysis of a  $\text{Ce}^{4+}$  salt at a very low pH in 1987,<sup>19a</sup> and Cabane et al. characterized their surface state after 6 years.<sup>19b</sup> Recently, Inoue et al. prepared a colloidal solution that consisted of 2 nm  $\text{CeO}_2$  nanocrystals via oxidation of cerium metal in 2-methoxyethanol under solvothermal conditions.<sup>22</sup> More recently, Niederberger et al. synthesized zirconia doped ceria nanoparticle sols by a combined method of hydroxide coprecipitation and sonication, using nitric acid as the peptizing agent.<sup>24</sup> However, the systematic investigation on the self-organization behavior of the colloidal  $\text{CeO}_2$  nanocrystals has been rarely reported.

In this paper, we present the synthesis of 4 nm  $\text{CeO}_2$  colloids via an alcohothermal method using poly(vinylpyrrolidone) (PVP) as the stabilizer and alkylamine (triethylamine, butylamine, or hexadecylamine) as the base and study their complex self-organized monolayer patterns on copper grids (i.e., isolated particles, short chainlike, pearl necklace-like, and dendritic

\* Corresponding authors. Telephone and fax: +86-10-6275-4179. E-mail: yan@pku.edu.cn.

<sup>†</sup> State Key Lab of Rare Earth Materials Chemistry and Applications.

<sup>‡</sup> Electron Microscopy Laboratory.

alignments). The synthetic mechanism and self-organized behavior of these colloidal CeO<sub>2</sub> nanoparticles have been investigated in detail by X-ray diffraction (XRD), transmission electron microscopy (TEM), high-resolution TEM (HRTEM), ultraviolet visible (UV-vis) spectroscopy, dynamic light scattering (DLS), and infrared spectroscopy (IR). On the basis of these characterizations, possible interparticle interaction modes have been suggested to explain suchlike complex self-organization patterns exhibited by the as-obtained CeO<sub>2</sub> nanocrystals.

## Experimental Procedures

**Materials.** Cerous nitrate (Ce(NO<sub>3</sub>)<sub>3</sub>·6H<sub>2</sub>O, ≥99.0%), potassium hydroxide (KOH, A. R. grade), butylamine (C<sub>4</sub>H<sub>9</sub>NH<sub>2</sub>, ≥99.0%), hexadecylamine (C<sub>16</sub>H<sub>33</sub>NH<sub>2</sub>, ≥92%), triethylamine ((C<sub>2</sub>H<sub>5</sub>)<sub>3</sub>N, ≥99.5%), poly(vinylpyrrolidone) (PVP, K30, Mw ≈ 30 000), ethanol (≥99.7%), and acetone (≥99.5%) were all used as received from Beijing Chemical Reagent Company, China.

**Synthesis.** Ce(NO<sub>3</sub>)<sub>3</sub>·6H<sub>2</sub>O (0.2 mmol) was dissolved in the PVP ethanol solution (40 mL, 10 to 30 g/L). Then, alkylamine (butylamine, hexadecylamine, or triethylamine, 2 mmol) was added into the Ce<sup>3+</sup> solution dropwise. After having been stirred for 10 min, the stock solution was transferred into a Teflon bottle with an inner volume of 50 mL. The bottle was held tightly in a stainless steel vessel and then heated in a temperature-controlled electric oven at 180 °C for 24 h under autogenous pressure. After being cooled to room temperature, the reaction solution was separated by filtration, and the CeO<sub>2</sub> colloid was thus obtained. The colloidal CeO<sub>2</sub> nanoparticles could be separated by adding an excess amount of water–acetone mixed solvent (v/v = 1:10) into the ethanol dispersion, and the thus-separated products could be easily redispersed in polar solvents such as water and methanol.

**Characterizations.** The TEM measurement was performed with a Philips Tecnai F30 FEGTEM operated at 300 kV or a JEOL 200CX at 160 kV. The HRTEM images were obtained on the Philips Tecnai F30 at 300 kV. The TEM and HRTEM samples were supported on carbon or Formvar-coated copper grids by dropping the as-prepared colloidal solutions under ambient conditions. The XRD patterns were recorded on a Rigaku D/MAX-2000 diffractometer with a slit of 1/2° at a scanning rate of 1° min<sup>-1</sup> using Cu Kα radiation (λ = 1.5406 Å). The samples were prepared by drying the obtained colloids at 80 °C in air overnight. IR spectra (4000–400 cm<sup>-1</sup>) of the ceria colloids were obtained on a Nicolet Magna 750 FTIR spectrometer at a resolution of 4 cm<sup>-1</sup> with a Nic-Plan microscope. UV-vis absorption spectra of the colloidal solutions were recorded on a Hitachi U-3010 spectrometer in a quartz cell (1 cm path length). Pure ethanol was selected as a blank. The optical absorption coefficient α was calculated according to the following equation:

$$\alpha = (2.303 \times 10^3 A \rho) / lc$$

where *A* is the absorbance of a sample, *ρ* is the real density of CeO<sub>2</sub> (7.28 g cm<sup>-3</sup>), *l* is the path length (cm), and *c* is the concentration of the CeO<sub>2</sub> nanocrystals (g cm<sup>-3</sup>). DLS experiments were carried out at 25 °C with ALV SLS-5022F laser light scattering spectroscopy and a Spectra-Physics 2017 Ar laser (514.5 nm wavelength). The scattering angle was 90°, and the intensity autocorrelation functions were analyzed by using the methods of CONTIN and cumulants. For the DLS measurements, the as-prepared colloidal solutions were centrifuged at 12 000 rpm for 30 min to remove the dust in advance.

## Results and Discussion

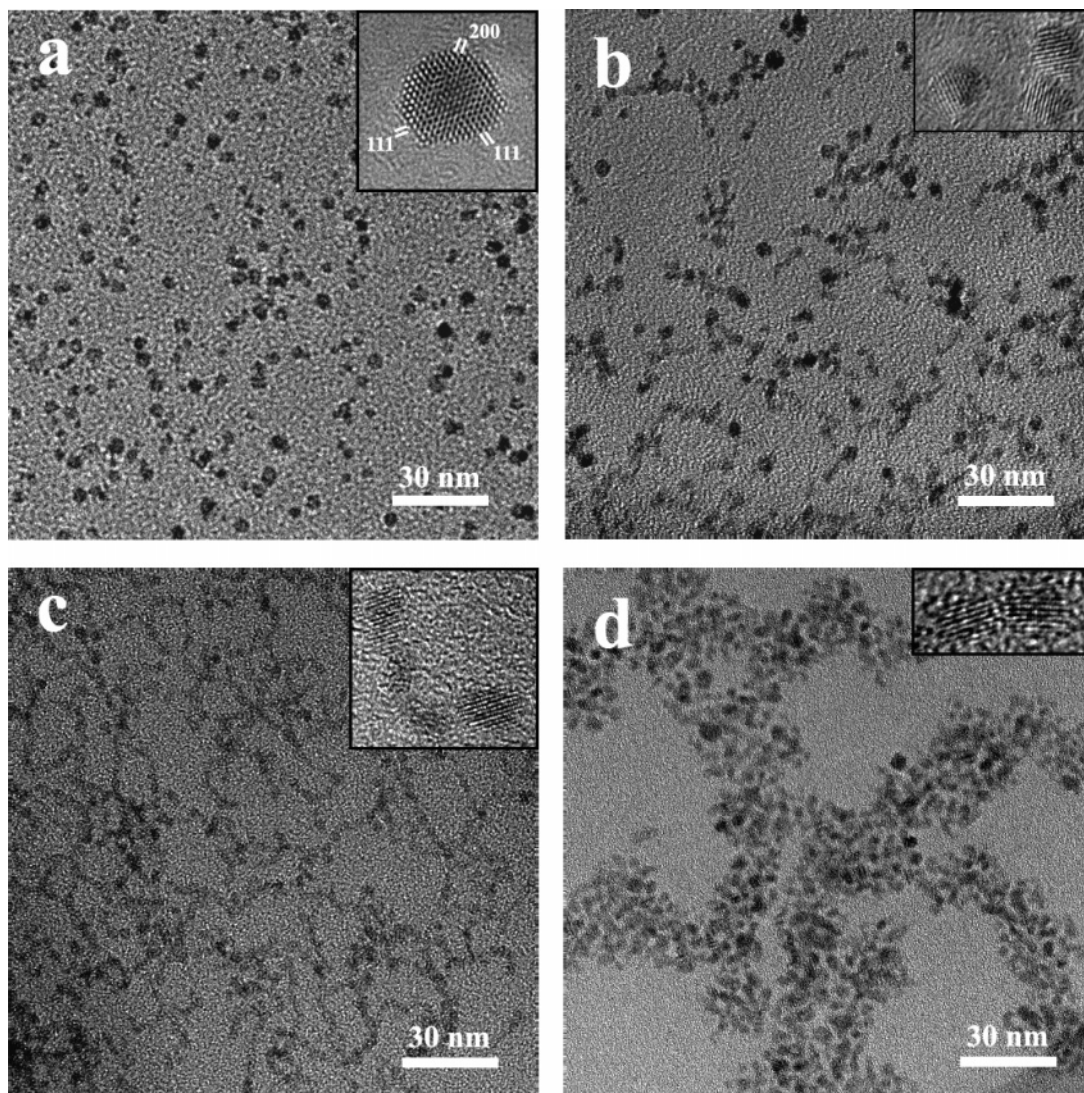
**Alcoholothermal Synthesis and Self-Organization Monolayers of CeO<sub>2</sub> Colloids.** Previously, aqueous dispersions of CeO<sub>2</sub> particles were prepared in a high concentration of nitric acid (pH = 0.5–2) with or without the aid of PVP.<sup>18–21,23,24</sup> Herein, our synthesis toward colloidal CeO<sub>2</sub> nanocrystals can be achieved under basic media in the ethanol solvent with an appropriate dielectric constant. All the CeO<sub>2</sub> colloids were transparent in yellow or orange (the characteristic color of Ce<sup>4+</sup> ion). After standing for several months under ambient conditions, the colloids showed high stability without any precipitates.

Figure 1 shows the TEM images of the samples synthesized using some typical alkylamines under different concentrations of PVP (*C*<sub>PVP</sub>). Interestingly, the CeO<sub>2</sub> colloids deposited on the copper TEM grids displayed various monolayer patterns including isolated particles (Figure 1a), short chainlike (Figure 1b, pseudo-1-D aggregated), pearl necklace-like (Figure 1c, 1-D aggregated), and dendritic (Figure 1d, pseudo-2-D aggregated) alignments, which are all composed of 4 nm nanoparticles. HRTEM images (insets in Figure 1) indicate that the obtained nanocrystals were of fluorite cubic structure (please also see the XRD pattern in Figure 1S) in the shape of polyhedra enclosed by the (111) and (200) crystal planes.<sup>25</sup> Figure 2 gives the dynamic behaviors for the as-obtained CeO<sub>2</sub> colloids in ethanol by DLS measurement. The mean sizes of the samples depicted in Figure 2 are obviously different from 17.0 to 73.2 nm, revealing the dissimilar aggregation status of the CeO<sub>2</sub>–PVP micelles in ethanol, which was strongly dependent on both the concentration of PVP and the variety of alkylamine employed in the synthesis.

On the basis of the present experiments and our previous research,<sup>26</sup> a tentative mechanism responsible for the formation of the CeO<sub>2</sub> colloids has been proposed and depicted in Scheme 1. Initially, the PVP molecule was adsorbed onto the solvated Ce<sup>3+</sup> ions in ethanol with the coordination between cerium cations and the oxygen atoms in PVP.<sup>20</sup> OH<sup>-</sup> ions were released by the hydrolysis of the dropped alkylamine, and water came from Ce(NO<sub>3</sub>)<sub>3</sub>·6H<sub>2</sub>O and ethanol (<0.2% H<sub>2</sub>O). Under such a basic condition, simultaneously, the oxidation transfer of Ce<sup>3+</sup> → Ce<sup>4+</sup> took place due to oxygen in air, and the color of the stock solution changed from colorless to light yellow.<sup>27</sup> The following alcoholothermal treatment afforded enough energy for the complete conversion of the Ce(OH)<sub>4</sub> nuclei into CeO<sub>2</sub> nuclei via dehydration and the subsequent growth of highly crystallized CeO<sub>2</sub> nanocrystals in the form of colloids, which were stabilized by PVP.

A series of condition-dependent experiments demonstrated that the introduction of PVP played double roles in the whole preparation. Above all, PVP greatly stabilized the as-formed Ce(OH)<sub>4</sub> nuclei and the as-obtained CeO<sub>2</sub> colloids via the bonding between its carbonyl groups and surface hydroxyls and simultaneously prevented them from self-aggregation via the repulsive forces arising from its hydrophobic carbon chains that extend into the solvents and interact with each other (steric hindrance effect). As a result, a steric barrier to the closer approach of the particles formed on the surfaces of the CeO<sub>2</sub> colloids. Figure 3a shows that tiny uniform particles were produced with the addition of PVP before alcoholothermal treatment with the corresponding weak SAED rings indicating their low crystallinity. In contrast, the sample prepared without PVP displayed stronger SAED rings as shown in Figure 3b, revealing the higher crystallized gellike materials. The adsorption of PVP effectively passivated the surface defects of the as-obtained CeO<sub>2</sub> nanocrystals and thus enhanced their UV





**Figure 1.** TEM images of the as-obtained  $\text{CeO}_2$  nanocrystals synthesized using (a) triethylamine,  $C_{\text{PVP}} = 30$  g/L; (b) triethylamine,  $C_{\text{PVP}} = 10$  g/L; (c) butylamine,  $C_{\text{PVP}} = 10$  g/L; and (d) hexadecylamine,  $C_{\text{PVP}} = 10$  g/L at  $180^\circ\text{C}$  for 24 h. Insets are their corresponding HRTEM images.

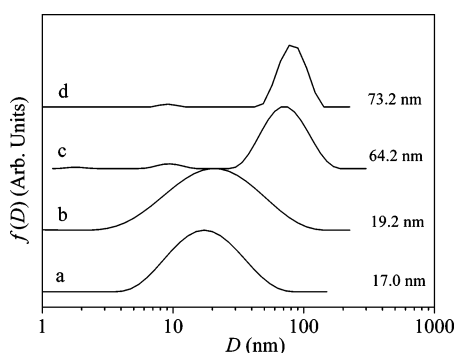
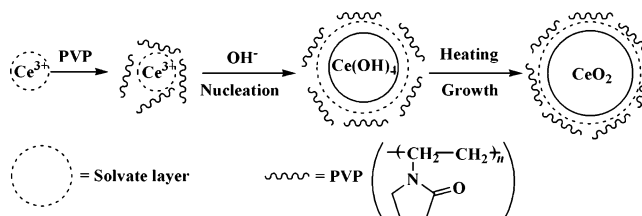


**Figure 2.** DLS size distributions of the as-obtained  $\text{CeO}_2$  colloids synthesized from (a) triethylamine,  $C_{\text{PVP}} = 30$  g/L; (b) triethylamine,  $C_{\text{PVP}} = 10$  g/L; (c) butylamine,  $C_{\text{PVP}} = 10$  g/L; and (d) hexadecylamine,  $C_{\text{PVP}} = 10$  g/L in ethanol at  $180^\circ\text{C}$  for 24 h.

absorption performance as depicted in Figure 4. For each curve, the band at ca. 300 nm is caused by the absorption of charge-transfer transition from O 2p to Ce 4f in  $\text{CeO}_2$ .<sup>28</sup> The absorption of colloidal  $\text{CeO}_2$  nanocrystals was significantly blue-shifted as compared with that of the aggregated counterparts, proving the good surface passivation effect of PVP.<sup>29</sup>

**Factors Affecting the Self-Organization Monolayers.** Four different self-organization monolayers appeared for our colloidal

#### SCHEME 1: Alcohothermal Mechanism for Synthesis of 4 nm Colloidal $\text{CeO}_2$ Nanocrystals



$\text{CeO}_2$  nanoparticles on the TEM grids and can be easily reproduced. In general, the aggregation of the colloidal nanoparticles on a substrate is largely dependent upon the following three factors: the surface-adsorption feature of the nanoparticles (nature and amount of the adsorbates), the type and surface state of the substrate, and the fabrication conditions (including the concentration of nanoparticles, ambient temperature, and humidity, etc.). In our experiments, we used copper grids coated with carbon or Formvar films as the substrates, and no noticeable substrate effect was found for the self-organized monolayer patterns of the studied  $\text{CeO}_2$  nanoparticles onto various copper grids. Moreover, we tried to keep the fabrication conditions the same for every TEM sample. Therefore, the previous multiple  $\text{CeO}_2$  self-organized patterns should be originated from the

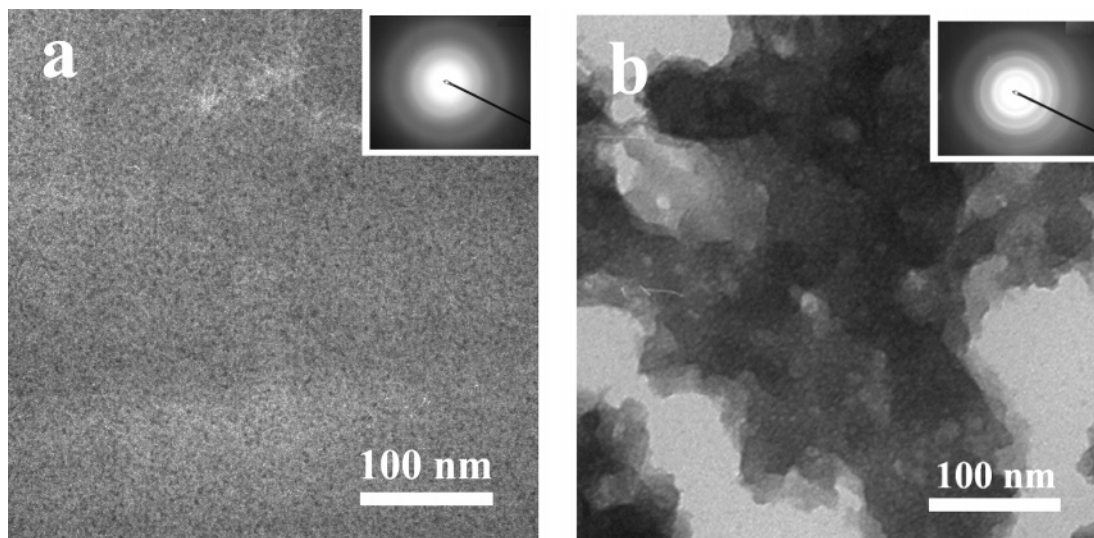


**Figure 3.** TEM images of the cerium samples synthesized using (a) triethylamine,  $C_{\text{PVP}} = 30$  g/L and (b) triethylamine,  $C_{\text{PVP}} = 0$  g/L before alcohothermal treatment. Insets are their corresponding selected area electron diffraction (SAED) patterns.

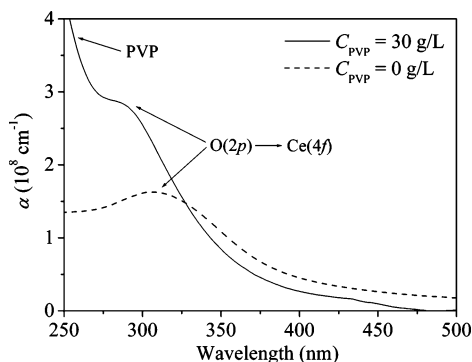


**Figure 4.** UV-vis absorption spectra of the as-obtained  $\text{CeO}_2$  synthesized using triethylamine and  $C_{\text{PVP}} = 30$  g/L (solid line) or 0 g/L (dotted line) in ethanol at  $180^\circ\text{C}$  for 24 h.

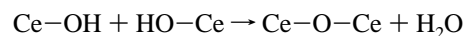
delicate balance of attractions and repulsions between the colloidal nanoparticles during the dynamic evaporation of the dispersant.<sup>3–8</sup>

**Surface Hydroxyls and PVP.** For simplification, we first used  $\text{Ce}(\text{NO}_3)_3$  and KOH (a fully ionized base) as the raw materials to prepare the  $\text{CeO}_2$  nanocrystals via the alcohothermal method without the addition of PVP. We observed that a large amount of brown precipitates, together with a clear upper solution, formed after the reaction. The brown precipitates are composed of severely aggregated  $\text{CeO}_2$  nanoparticles in random order (see Figure 2S). Figure 5a shows a pearl necklace-like aggregation pattern composed of the formed  $\text{CeO}_2$  nanoparticles as we dropped the upper colloidal solution onto the TEM grids. It demonstrates that the pearl necklace-like superstructure was the essential self-organization pattern for the colloidal  $\text{CeO}_2$  nanocrystals in the absence of PVP and alkylamine.

From Figure 5b,c, it can be clearly seen that the  $\text{CeO}_2$  nanoparticles aligned along one dimension and formed the pearl necklace-like pattern with some colloidal nanoparticles sharing the (111) or (200) planes with each other. This rare oriented aggregation may improve the efficiency for many types of devices and help the theoretical research on the physical and chemical properties under the nanometer domain.<sup>30</sup> Generally, the anisotropic 1-D assemblies of nanoparticles can be realized via multiple preparation methods of linear template, electric dipole moments, and oriented attachment, etc.<sup>30</sup> The present pearl necklace-like  $\text{CeO}_2$  aggregation can be explained by the

oriented attachment mechanism as suggested by Banfield et al.,<sup>31,32</sup> which involves spontaneous self-organization of adjacent particles so that they share a common crystallographic orientation, followed by the joining of these particles at a planar interface. During the oriented attachment, bonding between the particles reduces the total energy by removing surface energy associated with unsatisfied bonds.<sup>31,32</sup> This mechanism has been applied in many other metal oxide systems ( $\text{Fe}_2\text{O}_3$ ,<sup>33</sup>  $\text{TiO}_2$ ,<sup>31,34</sup>  $\text{SnO}_2$ ,<sup>35</sup> etc.).

There were three main ionic species ( $\text{K}^+$ ,  $\text{OH}^-$ , and  $\text{NO}_3^-$ ) inside the as-obtained colloidal  $\text{CeO}_2$  solution without the addition of PVP. The  $\text{K}^+$  cation and  $\text{OH}^-$  anion were produced by the ionization, while the nitrate anion came from  $\text{Ce}(\text{NO}_3)_3 \cdot 6\text{H}_2\text{O}$ . Under the basic conditions, the  $\text{OH}^-$  ions were predominately adsorbed onto the surface of  $\text{CeO}_2$  instead of  $\text{NO}_3^-$ , giving rise to the existence of a large portion of surface hydroxyls for the obtained  $\text{CeO}_2$  nanocrystals. The oriented aggregation was caused by the attraction from the elimination of surface hydroxyls on the adjacent particles via a condensation reaction dehydration between two surfaces under basic conditions,<sup>19b</sup> which can be simplified as



A part of the  $\text{CeO}_2$  nanocrystals even fused to each other by facets and grew as a whole (see the arrows in Figure 5c). This phenomenon is somewhat different from the report by Spalla et al., who obtained tenuous aggregates consisting of 5–10 nm  $\text{CeO}_2$  particles in the acidic medium by the assistance of a nitrate anion and PVP.<sup>20</sup> If we dropped nitric acid into our upper clear  $\text{CeO}_2$  ethanol dispersions to neutralize the surface hydroxyls in the absence of PVP, brown precipitates appeared immediately due to the severe aggregation of the  $\text{CeO}_2$  nanoparticles in the acidic medium.

When we started the synthesis just from  $\text{Ce}(\text{NO}_3)_3$  and KOH, most of the products precipitated after the reaction. This indicates that the electrostatic repulsion originating from surface hydroxyls cannot counteract the van der Waals attractions between the  $\text{CeO}_2$  nanoparticles. When PVP was added, a  $\text{CeO}_2$  colloid was obtained without precipitates. As shown in Figure 6a,b, the as-obtained nanoparticles spontaneously aggregated to the pearl necklace-like pattern on the TEM grids. As compared with Figure 5a,b, the relatively blurrier images indicate



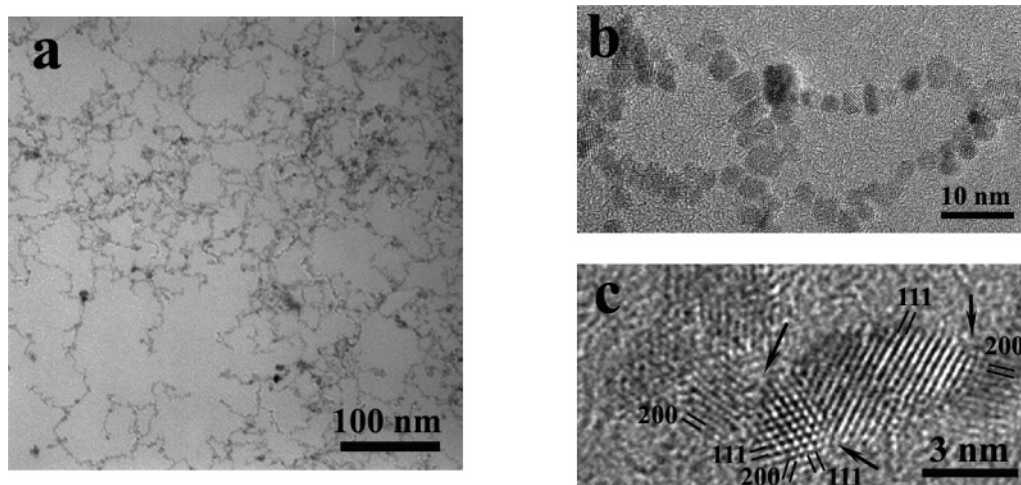


**Figure 5.** Low magnification (a) and high magnification TEM (b), and HRTEM (c) images of the as-obtained  $\text{CeO}_2$  colloid synthesized using  $\text{Ce}(\text{NO}_3)_3$  (5 mmol) and KOH (20 mmol) in ethanol at 180 °C for 24 h, without the addition of PVP.

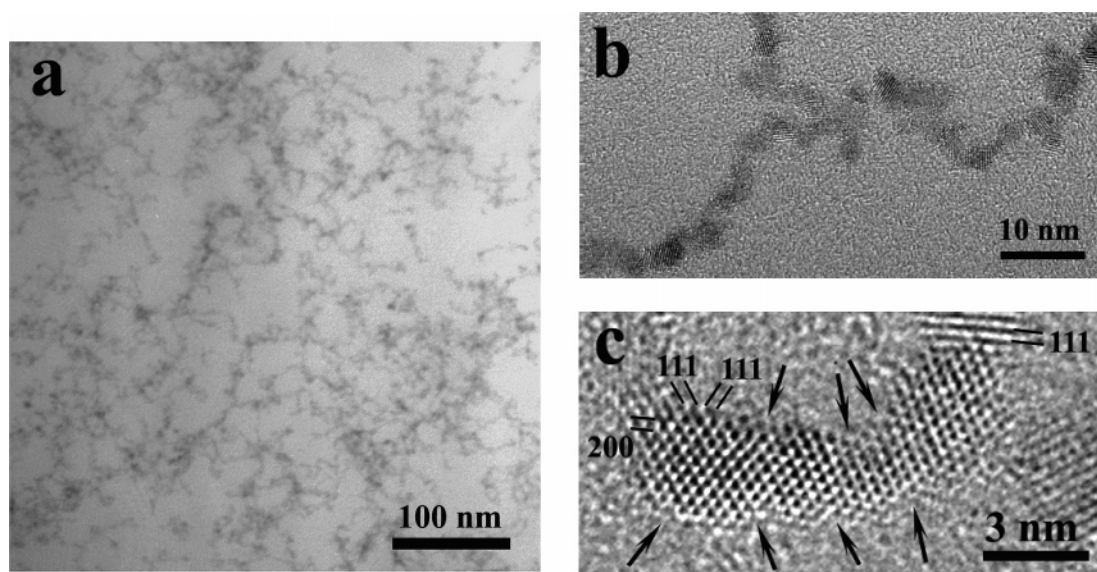


**Figure 6.** Low magnification (a) and high magnification TEM (b) and HRTEM (c) images of the as-obtained  $\text{CeO}_2$  colloids synthesized using  $\text{Ce}(\text{NO}_3)_3$  (5 mmol), KOH (20 mmol), and PVP (30 g/L) in ethanol at 180 °C for 24 h.

**TABLE 1: Numbers of Fused Nanoparticles by Sharing Different Facets for  $\text{CeO}_2$  Samples**

$C_{\text{PVP}}$ (g/L)	0	30
{100}	4 <sup>a</sup>	3
{110}	0	1
{111}	9	27
Total	13 (96 <sup>b</sup> )	31 (116)

<sup>a</sup> Statistic from the HRTEM images. <sup>b</sup> Number of the total investigated nanoparticles.

that PVP was truly adsorbed onto the surfaces of the colloidal  $\text{CeO}_2$  nanoparticles (also see the IR spectra in Figure 3S). However, the steric hindrance effect of PVP was relatively weaker than the oriented aggregation caused by the condensations between surface hydroxyls. Hence, the colloidal  $\text{CeO}_2$  nanoparticles maintained the pearl necklace-like monolayer pattern.

Figure 6c shows that a part of the  $\text{CeO}_2$  nanocrystals can further grow into single crystalline nanowires via fusing of their facets, just as in the cases of CdTe<sup>36</sup> and PbSe.<sup>37</sup> Table 1 shows that 31 out of 116 (27%) particles fused for the as-obtained  $\text{CeO}_2$  with the addition of PVP ( $C_{\text{PVP}} = 30$  g/L), while 13 out of 96 (14%) particles fused for the sample without PVP. It is a qualitative trend that PVP could favor relatively strongly

oriented aggregations. Normally, the strongly adsorbed stabilizer prevents the aggregation between colloidal nanoparticles due to its steric hindrance effect (so-called bumper effect of polymers in the colloidal dispersion).<sup>20</sup> In our case, PVP was weakly adsorbed onto the surfaces of ceria nanocrystals and could play the bridge-linking role since PVP has a linear structure and multiple coordinating sites (carbonyls).<sup>20</sup> Considering that the hydrodynamic radius of the applied PVP is about 10 nm,<sup>20</sup> one PVP molecule linked several particles simultaneously, and the chance of collision between two particles increased (the so-called sticker effect of polymers in the colloidal dispersion).<sup>20</sup> As a result, more  $\text{CeO}_2$  nanocrystals fused, and the oriented aggregation was enhanced by the addition of PVP.

From Table 1, it can be clearly seen that the number of fused  $\text{CeO}_2$  particles varied greatly during the oriented aggregation as the shared facets changed ({100}, {110}, or {111}). For the  $\text{CeO}_2$  nanocrystals synthesized from KOH and  $C_{\text{PVP}} = 0$  or 30 g/L, the observed frequencies of the shared facet that we have identified follow the same order in both cases: {111}  $\gg$  {100}  $>$  {110}. The {111} facets have the highest stability, or the lowest surface energy, among the previous three facets in  $\text{CeO}_2$ , according to the theoretical calculation.<sup>38</sup> Therefore, the least adsorbates (hydroxyls, PVP, etc.) settled on the {111} facets

of the colloidal  $\text{CeO}_2$  nanocrystals, and the most probable scenario for the particles were that they contacted and fused each other by  $\{111\}$ .<sup>35</sup>

As shown in Figure 1a, the isolated  $\text{CeO}_2$  pattern can be obtained when the concentration of PVP was increased from 10 to 30 g/L and triethylamine was used as the base. The mean size of the sample (Figure 2) synthesized from  $C_{\text{PVP}} = 30$  g/L was 17.0 nm that was slightly smaller than that synthesized from  $C_{\text{PVP}} = 10$  g/L (19.2 nm). It can be seen that the PVP stabilizer can exhibit its steric hindrance effect when triethylamine acted as the base.

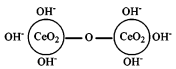
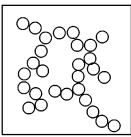
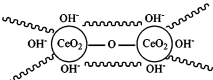
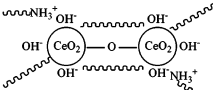
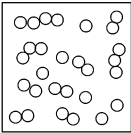
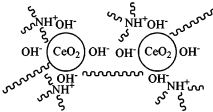
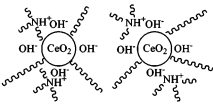
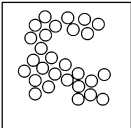
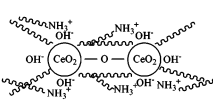
**Alkylammonium Cation.** When alkylamine was used as the base, various aggregated patterns of the colloidal  $\text{CeO}_2$  nanocrystals formed (see Figure 1). There were two kinds of species that may be adsorbed onto the surfaces of the nanoparticles besides hydroxyls and PVP: the residual alkylamine and the alkylammonium cation released by the hydrolysis of alkylamine. Considering that the coordinating ability of alkylamine to the cerium ion is much weaker than that of hydroxyl, the adsorption of alkylamine should be very weak (also see the IR spectra in Figure 3S), while the alkylammonium cation can strongly bond to the hydroxyl anion on the  $\text{CeO}_2$  surface with the electrostatic attraction. So we focused on the effect of the alkylammonium cation.

In experiments, the pearl necklace-like and short chainlike patterns appeared for the colloidal  $\text{CeO}_2$  nanocrystals synthesized from butylamine and triethylamine with the addition of 10 g/L PVP, respectively (also see Figure 1), indicating that the adsorption of the alkylammonium cation can change the self-organization behavior of the  $\text{CeO}_2$  nanoparticles under certain conditions. Butylammonium ion is a slim cation and has a weak steric hindrance effect. As shown in Figure 1c, the oriented aggregation remained when KOH was replaced by butylamine. In opposition, the triethylammonium ion is a plump cation and has a strong steric hindrance effect. Figure 1b shows that the aggregated pattern was changed to the pseudo-1-D short chainlike one as KOH was replaced by triethylamine. The mean size of the sample synthesized from triethylamine was 19.2 nm that was much smaller than that synthesized from butylamine (64.2 nm), as shown in Figure 2. All the previous results reveal that the type of alkylamine, essentially the steric hindrance effect, had a great influence on the aggregated pattern of the colloidal  $\text{CeO}_2$  nanocrystals.

In geometry, the pseudo-2-D dendritic pattern resembles the 1-D pearl necklace-like one but has a broader width. As for our  $\text{CeO}_2$  nanoparticles, the dendritic self-organized monolayer was produced when hexadecylamine, a long-chain alkylamine, was selected as the base (see Figure 1d). It can be explained that the hydrophobic interaction between PVP and flexible carbon chain in hexadecylamine enlarged the volume of the  $\text{CeO}_2$ -PVP micelles, and the nanoparticles were packed tightly to give the dendritic pattern. As shown in Figure 2, the mean size of the  $\text{CeO}_2$  sample synthesized from hexadecylamine was 73.2 nm that was larger than that from butylamine (64.2 nm). It indicates that the introduction of hexadecylamine increased the aggregation degree of PVP- $\text{CeO}_2$  micelles in ethanol and thus led to the formation of the dendritic self-organized pattern on the TEM grids.

**Self-Organization Mechanism of the Nanosized  $\text{CeO}_2$  Colloids.** For nanosized colloidal particles, self-organization driven under the reduction of total energy for the whole particle system takes place naturally but in a complex manner.<sup>30</sup> The monolayer pattern of the self-organization on a substrate is the direct result of the delicate balance of the attractive and repulsive

## SCHEME 2: Possible Mechanism Accounting for Formation of Various Self-Organized Monolayer Patterns for As-Obtained 4 nm $\text{CeO}_2$ Nanoparticles

Reaction system	Aggregated pattern	Possible interparticle interaction
$\text{Ce}(\text{NO}_3)_3 + \text{KOH}$		
$\text{Ce}(\text{NO}_3)_3 + \text{KOH} + \text{PVP}$ (30 g/L)		
$\text{Ce}(\text{NO}_3)_3 + \text{butylamine} + \text{PVP}$ (10 g/L)	Pearl necklace-like	
$\text{Ce}(\text{NO}_3)_3 + \text{triethylamine} + \text{PVP}$ (10 g/L)		
$\text{Ce}(\text{NO}_3)_3 + \text{triethylamine} + \text{PVP}$ (30 g/L)	Isolated	
$\text{Ce}(\text{NO}_3)_3 + \text{hexadecylamine} + \text{PVP}$ (10 g/L)		
<p>○ = 4 nm <math>\text{CeO}_2</math> nanoparticle    ~~~~~ = PVP    ~~~~~ <math>\text{NH}_3^+</math> = Butylammonium cation</p> <p>~~~~~ <math>\text{NH}_3^+</math> = Triethylammonium cation    ~~~~~ <math>\text{NH}_3^+</math> = Hexadecylammonium cation</p>		

forces between colloidal nanocrystals under its deposition condition. In the present research, we can controllably achieve four self-organized patterns for the as-obtained colloidal  $\text{CeO}_2$  nanoparticles on the TEM grids by tuning the used base and concentration of PVP (Figure 1).

Considering that all of our  $\text{CeO}_2$  samples were synthesized under similar basic circumstances, the attractive forces from the condensation of the surface hydroxyls between adjacent particles should be in the same magnitude. For such  $\text{CeO}_2$  nanoparticles in considerably small sizes, the repulsive forces of all the adsorbed species ( $\text{OH}^-$ , PVP, and alkylammonium cation, etc.) between adjacent particles are relatively weak; thus, the oriented aggregation certainly occurs and the subsequent particle coalescence preferably generates chainlike superstructures (e.g., pearl-necklace-like, 1-D aggregated) via the condensation reaction of surface hydroxyls. The formation of the chainlike superstructures is governed by the oriented attachment mechanism,<sup>31,32</sup> just like the cases of  $\text{TiO}_2$  and  $\text{SnO}_2$  nanoparticles.<sup>34,35</sup> As the repulsive forces increase to some extent, short chainlike  $\text{CeO}_2$  clusters (pseudo-1-D aggregated) will form due to the considerable weakening of the 1-D-orientated aggregation. Furthermore, as the repulsive forces increase to be extremely large, the nanoparticles will be nearly isolated. According to these deductions, some interparticle interaction modes were proposed to account for the as-observed diverse self-organized monolayer patterns for our  $\text{CeO}_2$  nanocrystals as depicted in Scheme 2.

In those modes, the adsorption of more hydroxyls on the surfaces of CeO<sub>2</sub> nanoparticles favored the formation of a pearl necklace-like superstructure via the 1-D-oriented aggregation. The adsorption of PVP contributed doubly to both the isolated pattern by its strong steric hindrance effect (at high PVP concentration) and the pearl necklace-like one by its bridge-linking effect arising from its multiple coordinating sites via carbonyls (at a low PVP concentration). At a given PVP concentration, the electrostatically adsorbed triethylammonium cations can remarkably increase the total repulsive forces between adjacent particles owing to its steric hindrance effect, which tended to break the 1-D-oriented aggregation and in turn led to the formation of short-chain (pseudo-1-D aggregated) and even isolated monolayer patterns. In the case of hexadecylamine, the electrostatically adsorbed hexadecylammonium cations generated the dendritic pattern (pseudo-2-D aggregated) because of the increased attractions between 1-D aggregated particle chains arising from its hydrophobic interactions with the PVP micelles between carbon chains.

## Conclusions

We developed an alcohothermal method to prepare ceria colloids from the PVP stabilizer and the alkylamine base. The as-obtained colloids were composed of 4 nm CeO<sub>2</sub> nanocrystals in a cubic structure. The introduction of PVP not only effectively prevented the cerium nuclei from self-aggregation but also greatly eliminated surface defects of the as-obtained nanoparticles. Interestingly, the colloidal CeO<sub>2</sub> nanocrystals appeared as isolated, short chainlike, pearl necklace-like, or dendritic self-organized patterns on the copper TEM grids. These special self-organization behaviors (from isolated particle to 1-D and 2-D aggregated alignments) were correlated with the delicate balance of attractions and repulsions caused by the adsorbed hydroxyls, PVP, and alkylammonium cations on the surfaces of the nanocrystals. The present colloidal CeO<sub>2</sub> nanocrystals may have potential applications as an anti-ultraviolet reagent and optical coatings, etc.<sup>16,17</sup> because of their small sizes and good aqueous dispersibility. Furthermore, the shown diverse self-organized behaviors of these colloidal nanocrystals will provide new research subjects for the surface chemistry and physics of nanoparticulate materials.<sup>7,30</sup>

**Acknowledgment.** We gratefully acknowledge financial aid from the MOST of China (Grant 2006CB601104) and the NSFC (Grants 20571003, 20221101, and 20423005).

**Supporting Information Available:** XRD pattern of the dried CeO<sub>2</sub> colloids (Figure 1S), TEM image of the precipitated brown CeO<sub>2</sub> powder (Figure 2S), and IR spectra of the as-obtained CeO<sub>2</sub> colloids and PVP (Figure 3S). This material is available free of charge via the Internet at <http://pubs.acs.org>.

## References and Notes

- (1) Bruchez, M.; Moronne, M.; Gin, P.; Weiss, S.; Alivisatos, A. P. *Science* **1998**, *281*, 2013.
- (2) Chan, W. C. W.; Nie, S. M. *Science* **1998**, *281*, 2016.
- (3) Motte, L.; Billoudet, F.; Pileni, M. P. *J. Phys. Chem.* **1995**, *99*, 16425.
- (4) Yin, J. S.; Wang, Z. L. *J. Phys. Chem. B* **1997**, *101*, 8979.
- (5) Lin, X. M.; Jaeger, H. M.; Sorensen, C. M.; Klabunde, K. J. *J. Phys. Chem. B* **2001**, *105*, 3353.
- (6) Pohl, K.; Bartelt, M. C.; Figueroa, J.; Bartelt, N. C.; Hrbek, J.; Hwang, R. Q. *Nature* **1999**, *397*, 238.
- (7) Rabani, E.; Reichman, D. R.; Geissler, P. L.; Brus, L. E. *Nature* **2003**, *426*, 271.
- (8) Huie, J. C. *Smart Mater. Struct.* **2003**, *12*, 264.
- (9) Taleb, A.; Petit, C.; Pileni, M. P. *J. Phys. Chem. B* **1998**, *102*, 2214.
- (10) Kiely, C. J.; Fink, J.; Brust, M.; Bethell, D.; Schiffrin, D. J. *Nature* **1998**, *396*, 444.
- (11) Li, M.; Schnablegger, H.; Mann, S. *Nature* **1999**, *402*, 393.
- (12) Kašpar, J.; Fornasiero, P.; Graziani, M. *Catal. Today* **1999**, *50*, 285.
- (13) Kašpar, J.; Fornasiero, P.; Hickey, N. *Catal. Today* **2003**, *77*, 419.
- (14) Kudo, T.; Obayashi, H. *J. Electrochem. Soc.* **1975**, *122*, 142.
- (15) Steele, B. C. H. *Nature* **1999**, *400*, 619.
- (16) Patsalas, P.; Logothetidis, S.; Metaxa, C. *Appl. Phys. Lett.* **2002**, *81*, 466.
- (17) Li, R.; Yabe, S.; Yamashita, M.; Momose, S.; Yoshida, S.; Yin, S.; Sato, T. *Solid State Ionics* **2002**, *151*, 235.
- (18) Hsu, W. P.; Rönquist, L.; Matijević, E. *Langmuir* **1988**, *4*, 31.
- (19) (a) Chane-Ching, J. Y. *EP* **208580**, **1987**. (b) Nabavi, M.; Spalla, O.; Cabane, B. *J. Colloid Interface Sci.* **1993**, *160*, 459.
- (20) Spalla, O.; Nabavi, M.; Minter, J.; Cabane, B. *Colloid Polym. Sci.* **1996**, *274*, 555.
- (21) Spalla, O.; Kélicheff, P. *J. Colloid Interface Sci.* **1997**, *192*, 43.
- (22) Inoue, M.; Kimura, M.; Inui, T. *Chem. Commun.* **1999**, 957.
- (23) Shchukin, D. G.; Caruso, R. A. *Adv. Funct. Mater.* **2003**, *13*, 789.
- (24) Deshpande, A. S.; Pinna, N.; Beato, P.; Antonietti, M.; Niederberger, M. *Chem. Mater.* **2004**, *16*, 2599.
- (25) Wang, Z. L.; Feng, X. *J. Phys. Chem. B* **2003**, *107*, 13563.
- (26) Zhang, Y.-W.; Si, R.; Liao, C.-S.; Yan, C.-H.; Xiao, C.-X.; Kou, Y. *J. Phys. Chem. B* **2003**, *107*, 10159.
- (27) Hirano, M.; Kato, E. *J. Am. Ceram. Soc.* **1996**, *79*, 777.
- (28) Zaki, M. I.; Hussein, G. A. M.; Mansour, S. A. A.; Ismail, H. M.; Mekhemer, G. A. H. *Colloids Surf. A* **1997**, *127*, 47.
- (29) Yang, C. L.; Wang, J. N.; Ge, W. K.; Guo, L.; Yang, S. H.; Shen, D. Z. *J. Appl. Phys.* **2001**, *90*, 4489.
- (30) Tang, Z.; Kotov, N. A. *Adv. Mater.* **2005**, *17*, 951.
- (31) Penn, R. L.; Banfield, J. F. *Science* **1998**, *281*, 969.
- (32) Banfield, J. F.; Welch, S. A.; Zhang, H.-Z.; Ebert, T. T.; Penn, R. L. *Science* **2000**, *289*, 751.
- (33) Penn, R. L.; Oskam, G.; Strathmann, T. J.; Searson, P. C.; Stone, A. T.; Veblen, D. R. *J. Phys. Chem. B* **2001**, *105*, 2177.
- (34) Oskam, G.; Nellore, A.; Penn, R. L.; Searson, P. C. *J. Phys. Chem. B* **2003**, *107*, 1734.
- (35) Leite, E. R.; Giraldo, T. R.; Pontes, F. M.; Longo, E.; Beltrán, A.; Andrés, J. *Appl. Phys. Lett.* **2003**, *83*, 1566.
- (36) Tang, Z.; Kotov, N. A.; Giersig, M. *Science* **2002**, *297*, 237.
- (37) Cho, K.-S.; Talapin, D. V.; Gaschler, W.; Murray, C. B. *J. Am. Chem. Soc.* **2005**, *127*, 7140.
- (38) Baudin, M.; Wójcik, M.; Hermansson, K. *Surf. Sci.* **2000**, *468*, 51.